Plasma Chemistry and Plasma Processing (2022) 42:535–559
https://doi.org/10.1007/s11090-022-10228-4

ORIGINAL PAPER

Air to H_2-N_2 Pulse Plasma Jet for In-Vitro Plant Tissue Culture Process: Source Characteristics

Kunpisit Kosumsupamala[1] · Phuthidhorn Thana[2] · Nattawut Palee[1] · Kantamard Lamasai[1] · Chakkrapong Kuensaen[3] · Athipong Ngamjarurojana[4] · Pranom Yangkhamman[5] · Dheerawan Boonyawan[1]

Received: 27 March 2021 / Accepted: 2 January 2022 / Published online: 4 February 2022

Abstract

Plasma agriculture has been considered as a promising solution for sustainable and safe agri-food production. Its applications include germination induction, plant-growth stimulation, post-harvest sterilization and management. For growth stimulation, both direct and indirect applications have been widely studied. For indirect plasma application, plasma-activated medium has largely been tested for its uses in plant management. This study preliminarily reports the diffusion pattern of plasma active radicals in semi-solid model and its effects on bacterial killing and plant tissue culture. A pulsed plasma jet with feeding gases of artificial air, ambient air, N_2, $H_2 + N_2$, H_2 and O_2 was used in this study. Results showed the generation and the deposition of inorganic ions of nitrogen—nitrate and ammonium—in the agar gel. Effects of feeding gases, medium softness, gas flow rate and activated-medium storage time on bacterial sterilization were also examined using *Escherichia coli* culture. The $H_2 + N_2$-treated medium showed the antimicrobial effects lasted for at least 60 min after the exposure. The distribution of RONS in the medium was visually examined by KI-starch chromogenic reaction and showed results relevant to the bactericidal effects. Effects of indirect plasma treatment on tissue culture shoot multiplication were also examined. Taken together, these results suggest that $H_2 + N_2$-treated media are a promising solution that can be widely used for economically important plant tissue cultures.

Keywords Pulsed plasma jet · Plasma-activated media (PAM) · Ammonium ion (NH_4^+) · In-vitro plant tissue culture

✉ Dheerawan Boonyawan
dheerawan.b@cmu.ac.th

[1] Plasma and Beam Physics Research Facility, Faculty of Science, Chiang Mai University, Chiang Mai 50200, Thailand

[2] Faculty of Science, Energy and Environment, King Mongkut's University of Technology North Bangkok, Rayong Campus, Rayong 21120, Thailand

[3] International College of Digital Innovation, Chiang Mai University, Chiang Mai 50200, Thailand

[4] Department of Physics and Materials Science, Faculty of Science, Chiang Mai University, Chiang Mai 50200, Thailand

[5] Faculty of Agricultural Production, Maejo University, Chiang Mai 50290, Thailand

Introduction

Cold atmospheric pressure plasma (CAP) has gained considerable attention in life-science scenarios. The richness of nitrogen (N_2) and oxygen (O_2) in ambient air interacts with non-equilibrium free electrons produced in the plasma source and leads to the formation of reactive oxygen and nitrogen species (RONS). RONS has been proposed to play a key role in biochemical pathways i.e. cell signaling and redox-balance regulation [1]. This opens up a broad spectrum of plasma applications, which can be divided into two aspects based on treatment procedures: direct and indirect treatments. First, the direct treatment allows cocktails of free electron, neutral and charged species, electric field, UV irradiation, short-lived and long-lived chemical species to reach and modify the target, for example, sterilization of medical devices [2], decontamination of SARS Covid-19 virus on surfaces [3], modification on polymer surfaces [4] and bacteria inactivation of plant seeds [5]. On the other hand, the indirect treatment is when plasma is first applied to a medium, which is then called the plasma-activated medium (PAM), before it is later applied to the sample. This is to benefit from further in-medium chemical reactions to produce a variety of final products. Therefore, tuning the properties of PAM paves a way to exponentially broaden the possibility of dynamic and complex plasma applications.

Plasma agriculture utilizes various plasma-induced products, which can be controlled for optimal range by operational parameters such as types of feeding gases, electrical power and treatment time. Especially, plasma-produced RONS has been proven to be a source of plant nutrients, including derivatives such as nitrite ion (NO_2^-), nitrate ion (NO_3^-), hydrogen peroxide (H_2O_2) and ammonium ion (NH_4^+) when applied as liquid solutions. Then, the treated solution is categorized as a type of PAM and called plasma-activated water (PAW). Studies showed the combination of plasma-assisted methods in a pre-harvest stage including seed direct treatment [5], PAW application on seeds [6], PAW irrigation [7] and indirect treatment on the hydroponic solution [8, 9]. However, few attentions have been paid to the plant tissue culture in which a part of plant tissue is cultured on a semi-solid media mixing with supplements. Although this environment-controlled technique provides a high production yield in favor of plant extraction, microbial hazards and nutrient deficiencies are required inconvenient and time-consuming regulation. This impractical issue sheds some light on promising characteristics of PAM which potentially address both effectively.

Drosera adelae (*D. adelae*) is a carnivorous plant in the genus *Dro*sera and the family Droseraceae. *Drosera* spp. are considered economically important ornamental plants and widely used in folk medicine for pulmonary diseases and coughs.The *Drosera* extracts contain bioactive compounds which are in the main group of flavonoids (e.g. quercetin, kaempferol), and naphthoquinones (e.g. plumbagin, ramentaceone) compounds in leaves and roots. These compound functions are antimicrobial properties and anti-cancer activity which are mostly used by the pharmaceutical, cosmetic and food industry [10, 11]. Fruitful potentials of *Drosera* extracts have drawn our attention to overcome the burdens of traditional plant tissue culture and the novel characteristics of PAM seem to be a promising solution.

In this study, a commercial-grade agar gel, which is the main component of plant tissue culture media, was directly treated with a COMPACT Air Plasma Jet device for 1 min. Air and a mixture of $H_2$75% + $N_2$25%(H_2 + N_2) gases were mainly focused as an effective source of NO_2^-, NO_3^-, H_2O_2 and NH_4^+ reported in previous works [12, 13]. The antimicrobial effects of plasma-treated gels were firstly characterized on *Escherichia coli* (*E. coli*) bacteria with different feeding gases and their plasma-chemical pathways were analyzed.

The effects of gel softness and flow rate of the plasma were subsequently investigated on sterilization area. Deposition of plasma-generated RONS inside the gel bulk was visualized by a well-known potassium iodide (KI)-starch reagent. The long-lasting properties of antimicrobial effects in plasma-modified gel were also studied. For plant nutrient promotion, the treatment of deionized (DI) water resulted in PAW and the concentrations of NO_3^-, H_2O_2 and NH_4^+ were examined spectroscopically. Finally, the results of plasma-stimulated effects on shoot multiplication of *D. adelae* were preliminarily investigated.

Experimental Methods

Plasma Characterization

Electrical Power Measurement

COMPACT Air Plasma Jet, which is a coaxial kHz-driven pulsed plasma source, was used in this work. The details of the device are described elsewhere [14]. Briefly, the burst repetition rate (BRR), which is defined as an inverse of one pulse period, was set to 20 kHz and the pulse width was 5.0 µs. Plasma treatment was operated for 1 min of treatment time with a total flow rate of 4 standard liter per minute (slm) by default. For the investigation of bacterial inactivation, gas flow rates were varied as 2, 4 and 6 slm. The gap distance, a distance between the plasma nozzle and the medium's surface, was fixed at 5 mm.

Feeding gases in this study were (1) artificial air (O_2 20% + N_2 80%), (2) air with relative humidity (RH) between 55 and 65%, (3) pure nitrogen (N_2), (4) a mixture of H_2 75% and N_2 25% (H_2 +N_2), (5) pure hydrogen (H_2) (6) pure oxygen (O_2). Noteworthy, higher hydrogen content or close to the stoichiometric ratio of ammonia (NH_3) could promote the formation of imidogen (NH) radicals since the average plasma electron density and temperature are increased [13], which is in favor of obtaining high ammonia productions.

The instantaneous electrical power $P(t)$ in a pulse of atmospheric pressure plasma discharge can be determined by measuring the voltage $V_x(t)$ at the high-voltage line via HV probe (P6015A; Tektronix, Inc., United States) as well as the current $I(t)$, which was deduced from the measured voltage across the 100-Ω resistor $V_y(t)$ by HV probe (T3100; Qingdao Hantek Electronic Co., Ltd., China). The V-I waveforms were recorded by a digital oscilloscope (TDS2014B; Tektronix, Inc., United States) as shown in Fig. 1a. Then, pulse-averaged electrical power P_{pulse} is calculated by:

$$P(t) = V_x(t)I(t) \tag{1}$$

$$P_{pulse} = \frac{1}{T}\int_t^{t+T} P(t)dt \tag{2}$$

where T is the period of a discharge pulse.

Optical Emission Spectra Measurement

Optical emission spectra (OES) were measured by a wide-spectrum spectrometer (Exemplar LS; B&W Tek, United States), which covers the range between 200–900 nm with a spectral resolution of 0.4 nm. The setup was carefully set along the plasma plume's axis

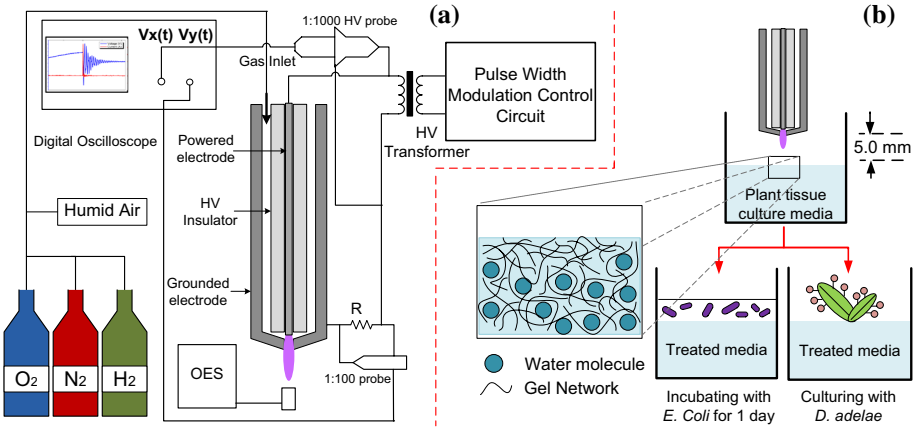

Fig. 1 **a** The schematic diagram shows a setup of electrical power using R = 100Ω and optical emission spectra (OES) measurements of the COMPACT Air Plasma Jet device operating with artificial air (O_2 20% + N_2 80%), humid air, pure nitrogen (N_2), a mixture of H_2 75% and N_2 25% (H_2 +N_2), pure hydrogen (H_2) and pure oxygen (O_2). **b** The diagram illustrates an overview of experimental procedures. The COMPACT Air Plasma Jet device was used to treat the agar-based tissue culture medium, a water-freezing-body model. The treated medium was then separately incubated with *E. coli* bacterium for the investigation of antimicrobial effects and used for the culture of *D. adelae*

to identify the emitted photons corresponding to transitions of plasma components in the plasma-active zone. Moreover, another short-range spectrometer (Avaspec ULS3648 Starline; Avantes, The Netherlands), which covers the range between 330–400 nm with a resolution of 0.035 nm, was also implemented. Since the 1-mm diameter size of the plasma nozzle is smaller than the fiber-optic probe, all collected spectra were plasma volume-averaged. All spectra were averaged for 5 samplings per measurement to increase a signal-to-noise ratio.

Gas Temperature Measurement

Gas temperature of the plasma was estimated from a thermal equilibrium between a plasma-treated glass plate and the plasma plume as described in our previous work [14]. The plasma nozzle was perpendicularly set to the 22 mm × 22 mm × 0.16 mm glass plate with the gap distance of 5 mm. A thermal imaging camera (FLIR ONE; FLIR Systems Inc., United States) was deployed to get a steady-state temperature with resolution of 0.1 °C. The initial temperature of the glass plate was approximately 25 °C.

Bacterial Inactivation by Plasma Indirect Effects

First, the culture medium for *E. coli* was prepared from 3% w/v nutrient broth (NB) and varying concentrations of agar (0.5–3% w/v) in DI water, mixed thoroughly, autoclaved, poured onto culture dishes, and left to set at room temperature.

Escherichia coli (TISTR 527) was obtained from Thailand Institute of Scientific and Technological Research (TISTR). The bacterium was grown until the bacterial density reaching 1×10^7 to 1×10^8 colony forming unit (CFU)/ml and, then, serial-diluted to 10^{-3} and kept at 4 °C.

The prepared nutrient agar was then exposed to plasma for 1 min with varying conditions: types of feeding gases (artificial air, ambient air, N_2, H_2 +N_2,H_2,O_2) or gas flow rates (2, 4, 6 slm).

A hundred microliters of prepared *E. coli* cell solutions were spread onto each dish of plasma-treated nutrient agar using an L-shaped glass spreader immediately after the plasma treatment or 5–60 min after the treatment (storage times). Then, the culture dishes were incubated at 37 °C for 24 h before being photographed. Area of bacterial inactivation or clear zone was measured by ImageJ software. Experiments were done in triplicate.

RONS Diffusion Pattern Examination in Agar Mixed with KI-Starch

KI-starch agar preparation procedure was adapted from Kawasaki et al. [15]. In brief, commercial-grade agar powder is dissolved in 25-ml of DI water, resulting in 0.5% weight by volume (w/v) concentration. Analytic-grade potassium iodide (KI) powder (Sigma-Aldrich, Germany) and starch soluble GR for analysis (Merck, Germany) were then added to reach 0.5% w/v. The solution was then autoclaved. KI-starch agar solution was left to set at the room temperature before further experiments.

KI-starch agar was then plasma-treated with varying feeding gases, (1) H_2 (2) H_2 +N_2 (3) N_2 (4) air for 1 min. After that, pictures were taken at different standing times (0–60 min) from both top and cross-section angles. The diffused area was measured.

Effects of Indirect Plasma Treatment on *Drosera adelae* Shoot Multiplication

½ VW medium was prepared from VW nutrient composition [16] supplemented with sucrose (final concentration of 10 g/l) and coconut water (final concentration of 75 ml/l). The pH of medium was adjusted to 5. Then, activated charcoal was added to reach the final concentration of 1 g/l and 9 g of agar was added to the final volume of 1 l prior to autoclaving at 121 °C for 20 min. The medium was then cooled down and kept at 25 °C.

Prior to culturing, the prepared agar was plasma-treated for 1 min with various feeding gases, 5-mm nozzle gap and a flow rate of 4 slm. After thorough sterilization, leaf explants of *Drosera adelae* were cut into pieces with approximate size of 1.0×1.5 cm. Then, the explants were placed on the pre-treated media. Each treatment had 5 replications. The explants were incubated under a 16-h photoperiod at 3,000 lx (Daylight LED tubes T8, 14 W) at 25 °C. The cultures were observed daily. The day of shooting and the number of shoots were recorded and analyzed.

Statistical Analysis

The one-factor analysis of variance (ANOVA) was applied to statistically analyze the effects of plasma treatments. Then, the results were analyzed by the Turkey's honestly significant difference (HSD) post-hoc test and the statistical significance were determined at $p<0.05$ (*), $p<0.01$ (**) and $p<0.001$ (***) accordingly.

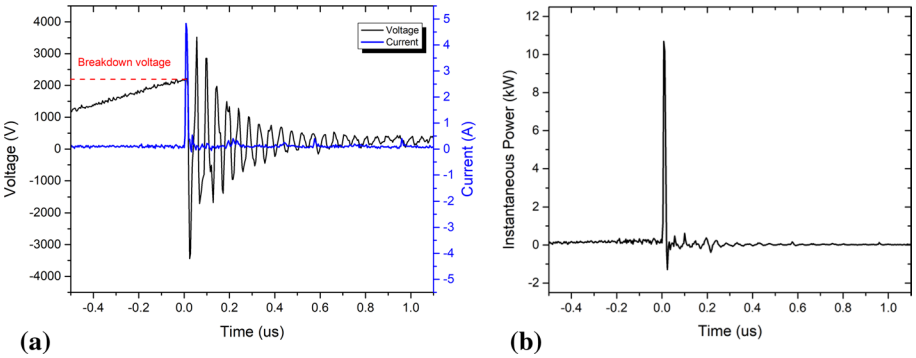

Fig. 2 **a** The synchronized current and voltage signals and **b** instantaneous power *P(t)* of the continuous pulsed mode of air plasma operated at atmospheric pressure illustrate the nano-discharge pattern

Table 1 Summary of electrical characteristics of the COMPACT Air Plasma Jet device operated in different feeding gases

	Artificial Air	Air	N_2	$H_2 + N_2$	H_2	O_2
$V_{breakdown}$(kV)	2.74 ± 0.04	2.67 ± 0.03	2.50 ± 0.04	2.05 ± 0.06	2.18 ± 0.02	2.62 ± 0.04
I_{peak}(A)	2.41 ± 0.13	1.98 ± 0.05	2.08 ± 0.07	0.77 ± 0.01	2.58 ± 0.09	2.82 ± 0.05
P_{pulse}(W)	0.96 ± 0.05	0.71 ± 0.02	0.80 ± 0.04	0.24 ± 0.01	0.57 ± 0.01	0.98 ± 0.03

Results and Discussion

Plasma Characteristics

Figure 2a shows the time-synchronized plots between the current and voltage signals during the plasma discharge. The voltage increased gradually and reached the breakdown voltage which strongly depends on the feeding gas. After that, the peak of the current immediately appeared. Therefore, the instantaneous power can be calculated and depicted in Fig. 2b. The peak of instantaneous power was roughly 20 ns at full width at half maximum (FWHM) which was already described as a transient-spark discharge in our previous work [14]. Table 1 summarizes the electrical characteristics of the plasma when operated with various feeding gases and the electrical powers are plotted in Fig. 3a. The breakdown voltage was highest in artificial air with 2.74 ± 0.04 kV following by ambient air (2.67 ± 0.03 kV), O_2 (2.62 ± 0.04 kV), N_2 (2.50 ± 0.04 kV), H_2 (2.18 ± 0.02 kV) and $H_2 + N_2$ mixture (2.05 ± 0.06 kV) respectively. The feeding-gas dependent trend was consistent with Paschen curves reported in other works [17, 18]. The pulse-averaged electrical power of the O_2-N_2 contained gases including artificial air, air, O_2 and N_2 was generally in range of 0.71–0.98 W. Meanwhile, the relatively low breakdown voltages of H_2 resulted in a drop of electrical power to 0.57 ± 0.01 W. Apart from that, the lowest electrical power of 0.24 ± 0.01 W in $H_2 + N_2$ plasma was also caused by the low peak current. This phenomenon has been reported in low-pressure glow discharge plasmas and suggested to be due to the smaller cross section of H_2 in comparison with N_2, reductions of Penning ionization or secondary electronic emission coefficient [19, 20].

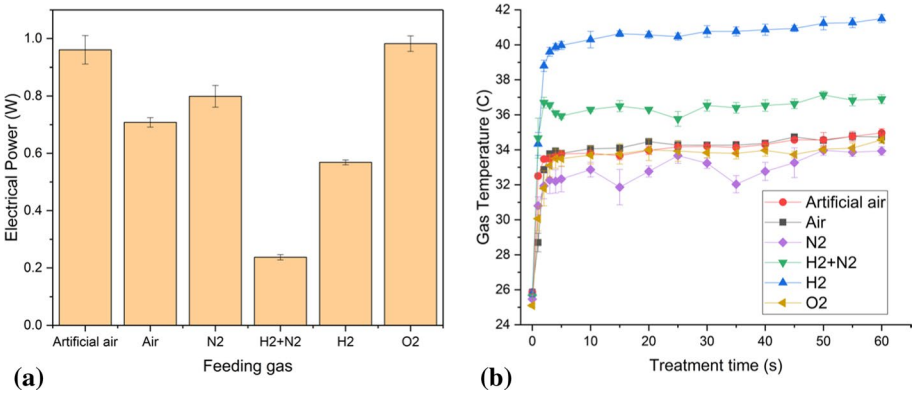

Fig. 3 **a** The electrical powers and **b** gas temperatures of the plasma operating with feeding gases deduced from the glass slide's temperature in the thermal equilibrium

Gas temperature is one of the crucial parameters that governs characteristics of the plasma chemistry leading to different pathways of RONS generation and destruction processes. The thermal-equilibrium temperature between the 5-mm gap plasma and the glass slide was obtained from the thermal imaging camera. During the 1 min of treatment time, all feeding gases showed a rapid increase of the temperature at first 5 s before reaching a steady state as illustrated in Fig. 3b. On the one hand, the group of air, artificial air and O_2 resulted in the almost identical temperature around 34.4 °C (34.3 ± 0.3 °C, 34.4 ± 0.3 °C and 34.5 ± 0.3 °C, respectively) while the slightly lower temperature of 33.4 ± 0.2 °C belonged to N_2 plasma. On the other hand, the temperatures of the H_2 and $H_2 + N_2$ plasmas rose to 36.4 ± 0.3 °C and 40.9 ± 0.3 °C after 1 min of treatment time. A significant increase of the gas temperature in H_2 plasma was also observed in Farouk et al.'s work and they reported that the ion Joule heating and Frank–Condon effect due to dissociation of H_2 were the main mechanisms of neutral gas heating [21]. On the other hand, the rise of gas temperature in $H_2 + N_2$ feeding gas is supposed to be the naturally exothermic reaction of gaseous NH_3 formation ($2N_{2(g)} + 3H_{2(g)} \rightarrow 2NH_{3(g)}$; $\Delta H = -92.44$ kJ/mol) [13]. However, the thermal effects were experimentally negligible since there was no melting of treated gels in all feeding gases.

The optical emission spectra of the plasma varying the types of feeding gases are shown in Fig. 4a. In the case of artificial air and (humid) air, the group of 2nd positive and 1st negative N_2 were dominated and there was also a relatively small peak of atomic oxygen O (777.4 nm). On the other hand, the spectrum of $H_2 + N_2$ mixture clearly showed the co-exist species of pure H_2 and pure N_2. Both H_α at 656.4 nm and H_β at 486.1 nm were observed in pure H_2. The N_2 feeding gas; meanwhile, only provided the group of 2nd positive and 1st negative N_2. Lastly, the dominant groups of atomic oxygen at 777.4 and 844.6 nm were detected together with a minority of 2nd positive and 1st negative N_2 in pure O_2 condition. To confirm the generation of NH which is the ammonia-derived radical, the spectrum of $H_2 + N_2$ was considered on the range of 330–360 nm. The result, which is illustrated in Fig. 4b, clearly showed the peak at 336 nm corresponding to NH formation.

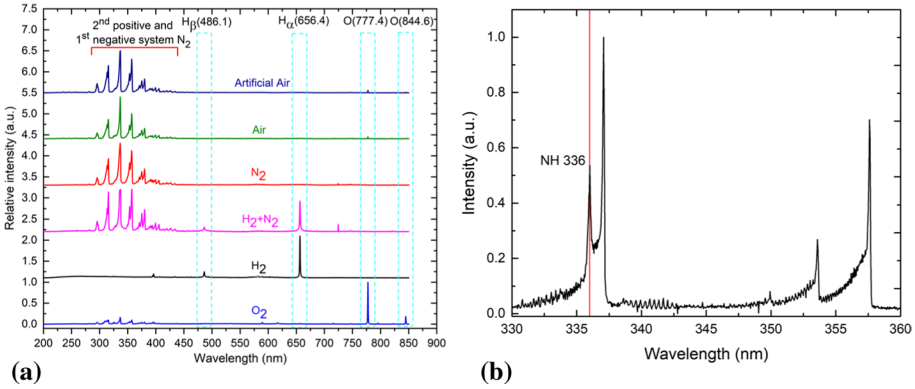

Fig. 4 **a** The optical emission spectra (OES) of the different plasma feeding gases including artificial air, air, pure N_2, $H_2 + N_2$, pure H_2 and pure O_2 in the plasma plume region. **b** An example emission spectrum of 75% H_2 and 25% $N_2(H_2 + N_2)$ plasma. Ammonia (NH_3) can be determined through the 336 nm emission of NH molecules produced via electron impact dissociation of ammonia

Factors Affecting Bactericidal Effect of the Plasma Treatment

Effect of Feeding Gas

Microbial inactivation is one of the most common applications of cold atmospheric pressure plasma. In agriculture, a wide range of plant diseases is caused by microorganisms. Thus, all tissue culture procedures and environments are needed to be sterilized. However, most sterilization methods affect the quality of the tissue culture medium. This led us to study the indirect plasma treatment on tissue culture medium. The tissue culture medium was treated with plasma for 1 min before spreading *E. coli* on the agar surface. Figure 5 shows the plasma-treated sample of *E. coli* bacteria on the 0.5% w/v agar gel. Plasma was operated 5-mm above the gel's surface and the different feeding gases were controlled at 4 slm of total flow rate. In case of pure gases, the killing zone was observed for H_2 and N_2 plasmas in the size larger than the plasma's nozzle but there was no observable clear zone in case of pure O_2.

At the surface of the gel, the transport of reactive species into the bulk of the gel involves many mechanisms such as plasma-induced pressure wave, charge interaction and diffusion [22, 23]. On the other hand, the majority of the agar gel is water, which is trapped by the network structure of agar [24, 25]. Therefore, it is reasonable to propose that the reactive species can penetrate through the semi-solid surface with a lower permeability factor and further react within the water inside the bulk of gel. We consider the agar gel as a static water body which is encapsulated by a thin elastic layer of polymer. The solubility of the gaseous species transporting through the water-containing gel's surface can be determined by Henry's coefficient which is exemplified in Table 2. The Henry's coefficient is a proportionality factor between the abundance of species in the gas phase to its abundance in the aqueous phase at equilibrium. Therefore, the possible chemical reactions were proposed on the basis of containing intermediates or products with a high Henry's coefficient.

Ozone (O_3) has been considered as a vital reagent for sterilization and bacterial inactivation. In the presence of oxygen in plasma active zone, the dissociation of gas-phase O_2 via electron impact takes place and forms atomic oxygen (O), which was clearly detected

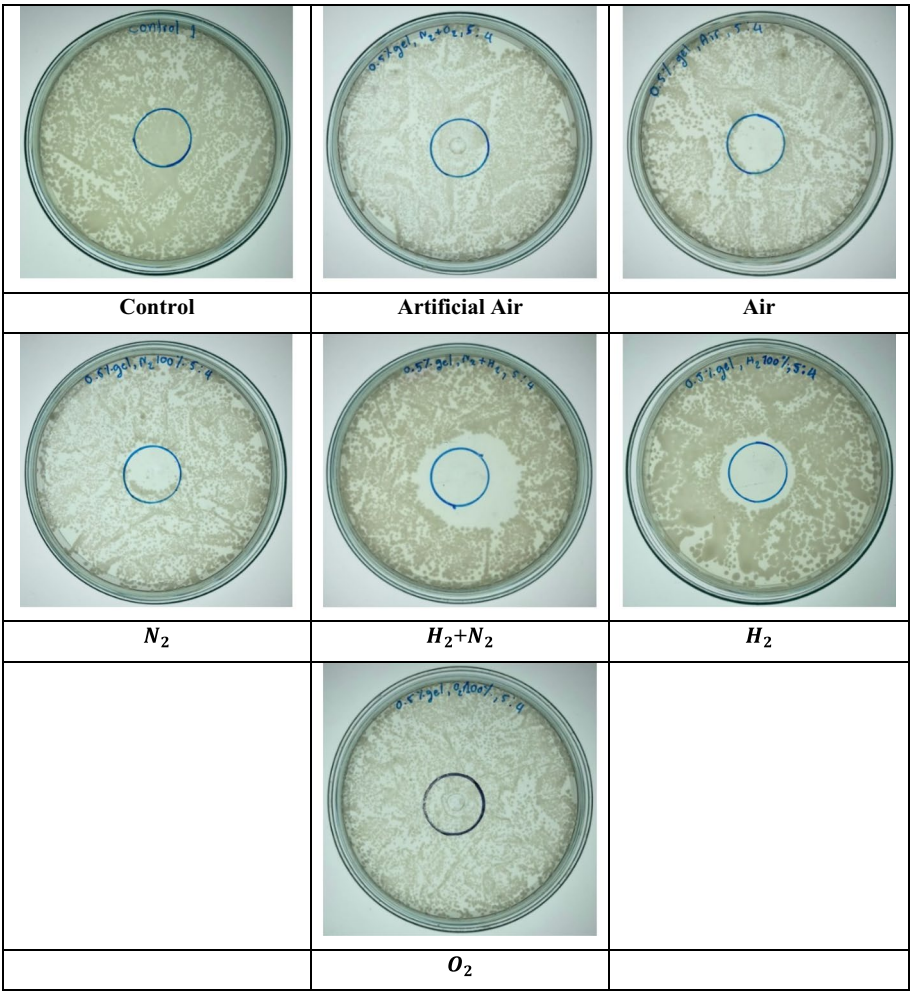

Fig. 5 Representative images of antimicrobial effects of plasma treatment with different feeding gases, as labeled in the figure, on *E. coli.* The nutrient agar was pre-treated with plasma for 1 min at a flow rate of 4 slm and 5-mm nozzle gap. The nutrient agars consisted of 0.5% w/v agar. Experiments were done in triplicate

in the optical emission spectra, in Reaction (S1). After that, the further reaction of O with surrounding O_2 results in the generation of O_3 as shown in Reaction (S2) In addition, the humidity in the ambient air also promotes the formation of hydroxyl radical (OH), hydrogen peroxide (H_2O_2) and hydroperoxyl radical (HO_2), which has been also reported to be effective in antimicrobial properties, in the gas phase by Reaction (S3)–(S5) [12, 26–28] (Figs. 6, 7).

The liquid-phase chemistry of O_2-derived species is listed in Reaction (S6)–(S9) [12, 26–29]. The major species in the liquid phase should be OH ($h_{OH} = 620$), HO_2 ($h_{HO_2} = 1.32x10^5$) and H_2O_2 ($h_{H_2O_2} = 1.96x10^6$). Then, the solvated O, OH, O_2,O_3, HO_2 and H_2O_2 react cyclically on each other and diffuse into the deeper zone. However, the formation of aqueous O_3 by Reaction (S8) is limited due to relatively low Henry's coefficients

Table 2 The Henry's coefficient of some plasma-produced RONS [26, 31–35]

Species	$h_{species}$(unitless)
HNO_3, O = NOOH	4.80×10^6
H_2O_2	1.96×10^6
HO_2	1.32×10^5
HO_2NO_2	9.73×10^4
H	6.00×10^3
NH	1.47×10^3
HNO_2, HNO	1.15×10^3
OH	620
N_2	600
N_2O_5	48.5
NO_3	41.8
H_2O	1
O	1
NO_2	0.28
O_3	0.274
NO	4.4×10^{-2}
O_2	3.24×10^{-2}
H_2	1.9×10^{-2}

of both reactants and product ($h_O = 1, h_{O_2} = 3.24x10^{-2}, h_{O_3} = 0.274$). This possibly leads to a small number of dissolved species in the gel's bulk which is mainly responsible for the antimicrobial effect. Although the O_3 has a long lifetime in the gas phase (~ hours to days) depending on environmental factors [30], its high reactivity only accounted for top-surface modification and led to the incapability of sterilization.

For the N_2-plasma, the dissociation of N_2 primarily produces atomic nitrogen (N) in the plasma active zone in Reaction (S10). Once the species transverses further in open air, the O_2-derived species come into play and can produce gaseous nitric oxide (NO) via Zeldovich mechanism (Reaction (S11)–(S12)), nitrogen dioxide (NO_2), nitrogen trioxide or nitrate (NO_3) and dinitrogen pentoxide (N_2O_5) (Reaction (S13)–(S16)). Subsequently, the gas-phase group of nitrous acid (HNO_2), nitric acid (HNO_3) and peroxynitric acid (HO_2NO_2) are formed by nitrogen oxides via a three-body reaction (Reaction (S17)–(S19)) and they are likely to be dominant species in the liquid phase of bulk gel due to their relatively high solubility ($h_{HNO_2} = 1.15 \times 10^3, h_{HNO_3} = 4.80 \times 10^6, h_{HO_2NO_2} = 9.73 \times 10^4$) [12, 26–28, 36].

The reactions of N_2-containing plasma with aqueous solution have been elaborately investigated [12, 26–28]. Apart from the solvation and solution of the aforementioned species, the production of nitrite ion (NO_2^-), nitrate ion (NO_3^-) and peroxynitrous acid ($O = NOOH$) can be formed in the liquid by Reaction (S20)–(S28) with the NO_X acting as intermediate species. Noteworthy, the formation of NO_2^- and NO_3^- in Reaction (S24)–(S27) results in acidity because of the presence of hydrogen ion (H^+) as well as hydronium ion (H_3O^+). Then, the NO_2^- with acidity can also decay to NO_3^- via Reaction (S28). This acidic condition with the presence of NO_2^- *and* H_2O_2 has been reported to be suitable for $O = NOOH$ formation which showed antimicrobial effect against *E. coli* suspension [12]. On the other hand, the decomposition of $O = NOOH$ possibly fuels the intermediate reactive species back to the chain pathways. Reaction (S29) accounts for 70% of $O = NOOH$

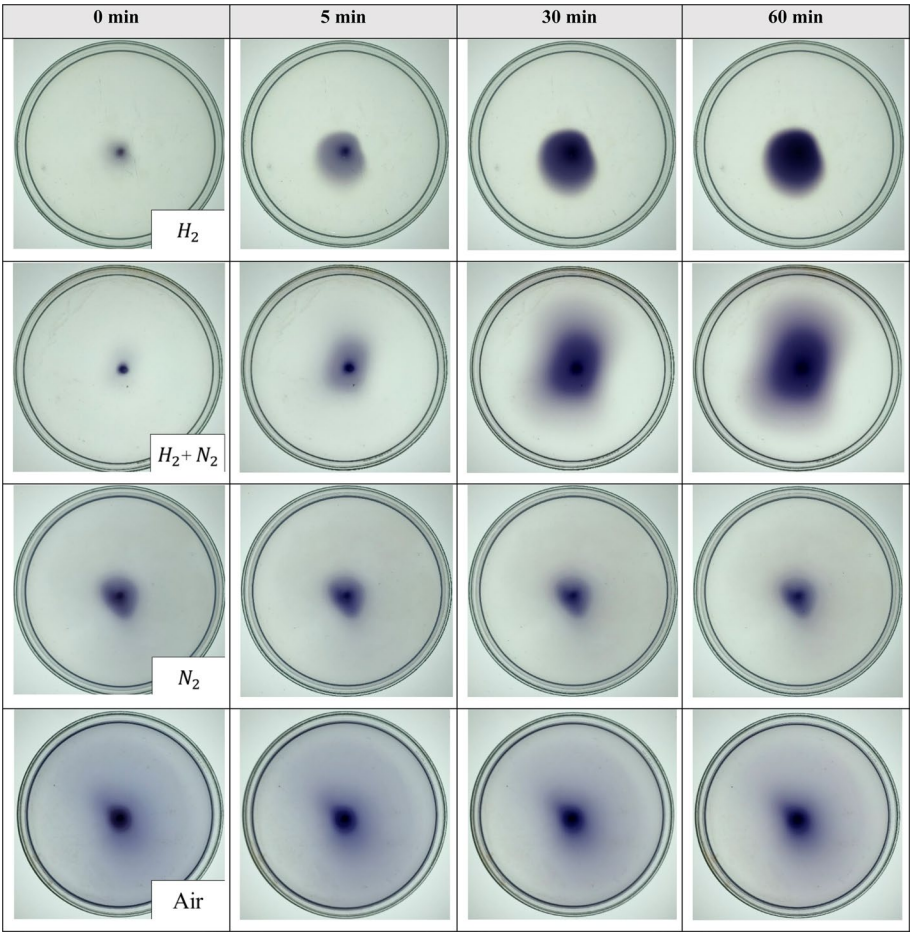

Fig. 6 Images of KI-starch agar after 1-min plasma treatment with different feeding gases—H_2, $H_2 + N_2$, N_2, and ambient air—and left for of 0, 5, 30 and 60 min (standing time). Experimental setting are as follows: 0.5% w/v agar, treatment gap = 5 mm, total flow rate = 4 slm. Experiments were done in triplicate

decay [37] which substantially relates to a detection of NO_3^-. The generation of H_2O_2 is likely to be attributed to OH radical produced by the remainder of $O = NOOH$ in Reaction (S30). These might be the explanation of the long-timescale of plasma-activated reactivity of the pure N_2 plasma.

In case of H_2-plasma, electron impact mainly dissociates the hydrogen gas (H_2) into atomic hydrogen (H) by means of Reaction (S31). The richness of gaseous H further reacts with the surrounding air containing O_2, N_2 and water vapor. Thanks to the relatively low molecular weight of H_2 compared to the air, an active zone of H_2-plasma is small and lets the air play a significant role in effluent's chemistry. An additional source of hydrogens is generated by the humidity through electron-impact in Reaction (S32)–(S34) [38]. The produced HO_2 possibly contribute gaseous H_2O_2 production through Reaction (S35)–(S37) but solvated H and H_2 might also decrease the amount of aqueous H_2O_2 via Reaction (S38)–(S39) [39]. The relatively large area of clear zone compared to the plasma nozzle was observed in our H_2-plasma experiment. We suggest that this antimicrobial effect is

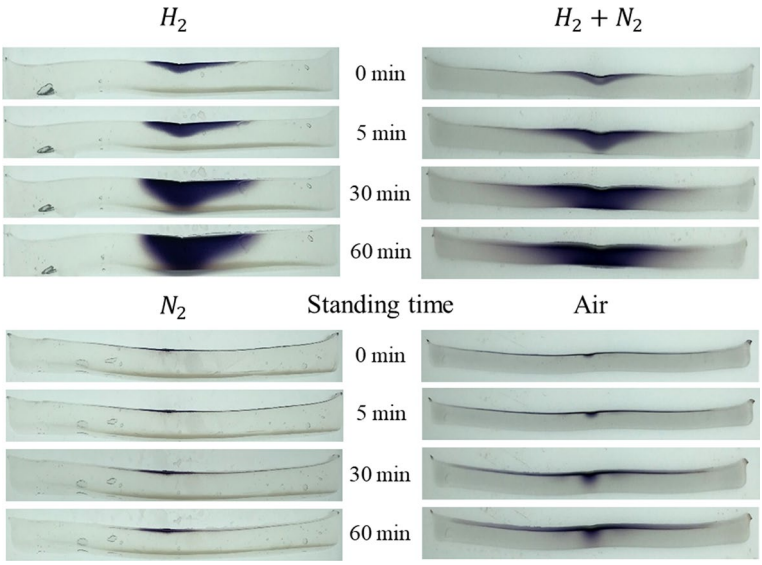

Fig. 7 Cross-section images of KI-starch agar exposed to 1 min of plasma treatment with H_2, H_2+N_2, N_2 or ambient air feeding gases at different standing times: 0, 5, 30 or 60 min. Experimental setting are as follows: 0.5% w/v agar, treatment gap = 5 mm, total flow rate = 4 slm. Experiments were done in triplicate

mainly dominated by H_2O_2 due to its high solubility ($h_{H_2O_2} = 1.92 \times 10^6$) and high diffusivity in water ($D_{H_2O_2} = 1.0 \times 10^{-9}$ m^2/s) [40].

Considering the comparison between humid air and artificial air (mixture of 20%O_2 and 80%N_2), the major difference in these conditions is the absence of humidity in feeding gas. Reuter et al. reported the contribution of humidity in feeding gas and shielding gas [38]. The results clearly showed a greater effect of increasing humidity in the feeding gas leading to a higher production rate of H_2O_2. They suggested that the main pathways were gas-phase Reactions of (S6) and (S32) in the core plasma. This could be an explanation of the survival of *E. coli* in case of artificially dry air. Moreover, chain reactions of liquid-phase chemistry are promoted by the presence of both oxygen and nitrogen-derived species indicated by the optical emission spectrum in Fig. 4a. The groups of NO_x and HNO_x species have been reported to be mainly produced together with O_3 and H_2O_2 and possibly lead to another chemical pathways by Reaction (S40)–(S43). The coexistence of various air-plasma species in solution has been accounted for synergic effects on bacteria-killing characteristics which could also be involved with pH, temperature and UV irradiation as well.

Interestingly, the mixture of H_2+N_2 gas indicated the largest clear zone compared to other gases which could be the hint for desirable species in antimicrobial treatment. The observation of *NH* spectra is expected to finally produce gaseous ammonia NH_3 according to Reaction (S44)-(S46). After that, hydrogen hydride species (*NH*, NH_2, NH_3) can transfer to the liquid, which is assumed to be *NH* form thanks to its Henry's coefficient ($h_{NH} = 1.47x10^3$), and result in aqueous form and ammonium ion (NH_4^+) (Reaction (S47)–(S50)) [13, 41]. These pathways clearly create more OH which is already described as a precursor of H_2O_2 creation. This chain of reaction is likely to take place in the *N*-abundance environment such as N_2 plasma with a small O_2-based interference compared to the artificial air. So, the bacterial inactivation of the N_2 plasma might be dominated by the H_2O_2 production via *NH*-derived species over the humidity suppression. It is reasonable

to propose that the presence of NH_4^+ increases the amount of aqueous H_2O_2 and causes the relatively large bacteria-free zone. To further investigate the deposition of plasma-induced RONS, KI-starch reagent, a RONS-induced chromogenic substrate, was applied to the nutrient-free agar in the following experiments.

Diffusion Pattern and the Deposition of Plasma-Generated RONS

In order to gain more information on the plasma-gel modification, the agar-based medium without nutrient broth was mixed with the KI-starch reagent before. The reagent has been widely used to visualize the distribution of plasma-produced RONS on the gel [15, 42, 43]. Due to the relatively low oxidative potential of iodine (I_2) compared to most of the RONS produced by the plasma, the abundance of iodide (I^-) deposited in the medium (Reaction (R1)) will give an electron to the presence RONS and turn into I_2 (Reaction (R2)). After that, the I_2 reacts with I^- to form triiodide (I_3^-) (Reaction (R3)) before leading to the complex formation with the starch (Reaction (R4)). However, emerging of the colored complex form is not selective but it is used to illustrate the overall distribution of reactive species in a single measurement.

To explore the diffusion of plasma-produced RONS on the target, the 1-min modified gels by the plasmas were cross-sectioned into the halves. The depth-direction profiles were then imaged at 0, 5, 30, and 60 min after the treatment as shown in Fig. 7. Obviously, the distributions of the H_2 and H_2+N_2 derived species were not only restricted on the surface, but also penetrated to the bulk of the gel. The diffusion and deposition process gradually took place from the surface accumulation at 0 min and reached the bottom side after 30 min corresponding to the darker top-view image. Lastly, the distribution at a very long-standing time of 60 min after modification showed the intensified zone mostly located in the gel's body.

Supplementarily, from the assumption that agar-based medium is a model of immobilized water, where agar structure only holds water molecules to place, DI water was exposed to plasma with various types of feeding gases to investigate the potential in-direct generation of active radicals. Concentration of hydrogen peroxide (H_2O_2), nitrate (NO_3^-) and ammonium (NH_4^+) radicals were measured by UV–Vis spectroscopy. However, since the experimental model was not comparable to the setting of agar-based media, the results were not included in the main text (Fig. S1). The preliminary results showed that the amount of H_2O_2 concentration was highest when treated with $H_2 + N_2$ plasma (6.821 ± 0.154 mg/l). This trend of detected H_2O_2 among feeding gases was in line with the observable size of the clear zones depicted in Fig. 5, which hints at the bactericidal characteristics of H_2O_2. The high concentrations of NO_3^- were also observed together with the increased H_2O_2 concentrations induced by the air plasma (4.532 ± 0.471 mg/l) and N_2 plasma (4.237 ± 0.470 mg/l), supporting the proposed pathways of O = NOOH decomposition or NO_x /HNO_x formation. NH_4^+ was also found in highest concentration when induced by $H_2 + N_2$ plasma (2.333 ± 0.412 mg/l). Up to this point, $H_2 + N_2$ plasma is a desirable treatment for the production of plant nutrients in DI water. Thus, the highly penetrable profiles from Fig. 7 potentially represent the collective behavior of NH_4^+ and diffusive H_2O_2.

Utilization of ambient air as a feeding gas for plasma generation is well-known for its high mobility and cost-effectiveness. The diffusion results of RONS produced from air plasma showed a strong horizontal distribution immediately after the treatment, while vertical distribution only localized at the treatment point. In comparison to N_2 plasma, this low-penetrable area is reasonably associated with NO_3^--related species such as NO_x which

mostly have a low Henry's coefficient. In addition, the presence of the point-like pattern in the air plasma may be due to higher amount of O or O_3-derived species. For example, direct formation of gaseous HNO_x and HO_2NO_2, which are high Henry's coefficient's species, through three-body collision (Reaction (S17)–(S19)). Uhm et al. studied the influence of oxygen in closed-system N_2 plasma jet treated on water [44]. They reported the peak of HNO_3 ($h_{HNO_3} = 4.80 \times 10^6$) density when the oxygen mole fraction was close to air composition ($\xi \sim 0.21$) while both NO ($h_{NO} = 4.4 \times 10^{-2}$) and HNO_2 ($h_{HNO_2} = 1.15 \times 10^3$) densities were higher in low oxygen condition ($\xi < 0.25$) like N_2 plasma. Moreover, the preliminary investigation on plasma-induced radical generation in DI water, though cannot be directly compared, gave useful insights. The increasing trend of NO_3^- and dramatic reduction of NH_4^+ with the increasing oxygen mole fraction were also consistent with our findings. However, our tendency of H_2O_2 was slightly different which is likely to be caused by the strong effects of feeding humidity in air plasma (Fig. S1). On the other hand, the broad distribution in the air plasma is highly suggested to be O_3 because of its high reactivity and long lifetime. These unique characteristics in the RONS penetration from 4 feeding gases are important information for the production of plasma-activated medium (PAM) with long-lasting effects. The presence of plant-nutrient derivatives in a single treatment along with antimicrobial effects of $H_2 + N_2$ treatment was desirable for the plant tissue culture. Hence, further study on the effects of medium softness and flowrate on antimicrobial activities will be focused on $H_2 + N_2$ plasma treatment in the next sections.

Effect of Medium Softness

Apart from the active radicals from plasma, the properties of the target are also considered important in substrate modification. Figure 8 illustrates the clear zone of *E. coli* settled on the gel treated with the H_2+N_2 gas plasma for 1 min before. The plasma was fixed at the gap of 5 mm above the gel with a total flow rate of 4 slm. The percentages of agar used to prepare the gel were varied as 0.5, 0.9 and 3% w/v which directly affect the softness of the sample. The results showed that the stiffer the sample, the larger the clear zone was observed. The area of the clear zone in the 0.5%w/v gel was 11.975 ± 0.355 cm^2 which was significantly different from both 0.9%w/v gel with 14.568 ± 0.681 cm^2 and 3.0%w/v gel with 15.724 ± 0.912 cm^2. We propose that the same amount of RONS is firstly produced in gas phase before depositing on the gel's surface. The degree of deposition of reactive species can be considered by penetration depth. A dense media prevents the transport of species in the depth direction and subsequently results in the broader distribution in the radial direction instead. Previous studies on gelatin gel showed a linear decrease of penetration depth as a function of gel mixing percentage [45, 46]. Xu et al. additionally showed the same trend in agarose gel. They suggested that the lower mixing percentage gel has more void spaces and higher permittivity which facilitates the movement of solute species [40].

Effect of Gas Flow Rate

Gas flow rate of plasma feeding gas also contributes to the delivery of plasma-generated reactive species to the target. Figure 9 shows the clear zones of *E. coli* on the 0.5% w/v gel treated with H_2+N_2 plasma with different flow rates—2, 4 or 6 slm—for 1 min. The most effective condition accounted for the flow rate of 6 slm corresponding to the clear zone area of 29.125 ± 0.686 cm^2. Meanwhile, the gels treated with 2-slm and 4-slm flow rates

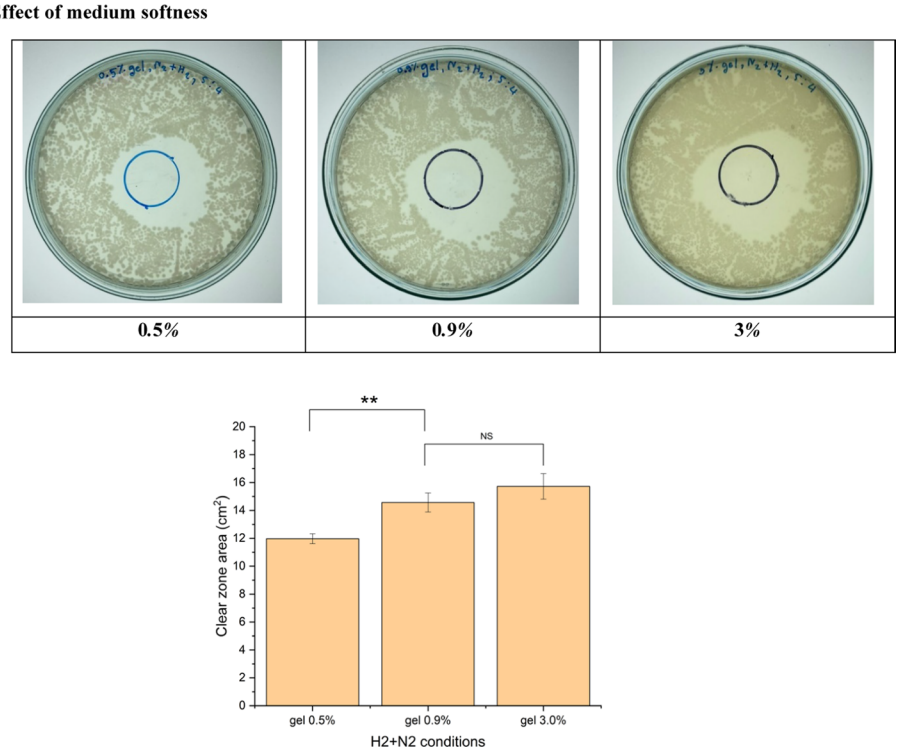

Fig. 8 Images of antimicrobial effects on the *E. coli* after treated gels by the H_2+N_2 gas plasma with the total flow rate of 4 slm for 1 min on 0.5, 0.9 and 3%w/v of agar gel. Quantitative measurement of the clear zones was shown below. NS, not significant. $*p<0.05$, $**p<0.01$, $***p<0.001$. The nozzle gap was set at 5 mm. Experiments were done in triplicate

resulted in not significantly different sizes of clear zone (9.623 ±0.534 cm^2 and 10.626 ± 0.778 cm^2) although the flow rate was doubled.

It has been widely known that the flow dynamics influence the RONS distribution in both plasma plume and afterglow regions. The pressure of feeding gas pushes on the surface at the treatment point and causes the radially outward flow during the plasma modification. The expansion of the clear zone as the increase of total flow rate, in which the larger number of particles containing momentums hits and functionalizes the surface, is unsurprised. However, the insignificant change of clear zone between the total flow rate of 2 and 4 slm compared with flow rate of 4 and 6 slm was observed. There are 2 possible factors that could explain this consequence. Firstly, the instability of flow, which is determined by Reynold's number and strongly depends on the geometry of the system, is likely to happen especially at the high speed of flow [47, 48]. The Reynold number of a tube with a diameter D(m) is expressed as $Re = v\rho D/\mu$ where v is the fluid velocity (m/s), ρ is the fluid density (kg/m^3) and μ is the kinematic viscosity of the fluid (kg/m s). The fluid velocity can be written in terms of the total flow rate Q (m^3/s) passing through cross-section area A (m^2) by $Q = Av = \pi(D/2)^2 v$. The viscosity of H_2+N_2 mixture = $1.205x10^{-5}$ kg/m s was obtained by the simple method proposed by Devidson

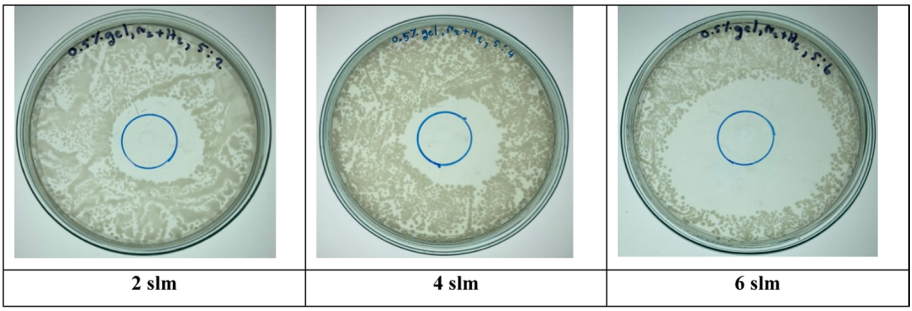

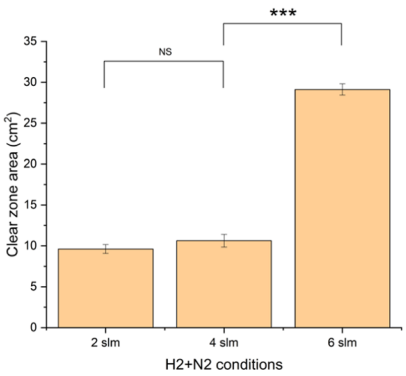

Fig. 9 Representative clear-zone images of *E. coli* on the 0.5% w/v gel treated with H_2+N_2 plasma with different flow rates—2, 4 or 6 slm—for 1 min. The nozzle gap was set at 5 mm. Quantitative measurement of the clear zones was shown below. NS, not significant. $*p<0.05$, $**p<0.01$, $***p<0.001$. Experiments were done in triplicate

[49] using the viscosity of $H_2 = 8.849x10^{-6}$ kg/m s and viscosity of $N_2 = 1.770x10^{-5}$ kg/m s at the room temperature. For the 1.0-mm diameter of the plasma nozzle, Reynold numbers of 2,4 and 6 slm were 2,421, 4,824 and 7,263 respectively. The results were in good agreement with general criteria of the flow regime which the transition between laminar and turbulent flows occurs around $2000 < Re < 4000$ and the turbulent flow takes place at $Re > 4000$. Secondly, the plasma-surface interaction could also be attributed to clear zone enlargement. Increasing total flow rate tended to increase a plasma plume length and contact with the gel's surface. Yue et al. studied OH and O distributions by the impingement of He plasma jet on glass, distilled water and metal substrates [50]. They observed the enhancement of gas-phase OH densities in conductive substrates (water and metal) which might be due to a restrike breakdown (third discharge). Moreover, the increased gas flow rate also promoted the radial expansion of OH distribution because the surface ionization wave can propagate further in the optimal mixture ratio of air. Another work of Simoncelli et al. demonstrated the role of conductivity and capacitance of substrates on impinging ns-pulse He plasma jet [51]. It was illustrated that the electrical properties of dielectric, liquid, metal samples are not only affected the electric field distribution, but also the flow dynamics. Therefore, our small

5-mm gap and the agar gel, which is considered as a hybrid of dielectric and conductor, can both influence the sterilization process.

Lasting Effect of the Generated RONS

The previous results gave the clue for the post-treatment effects of the plasma modification on the tissue culture medium. Many studies already showed the life science-related applications of plasma sterilization and decontamination by not only direct treatment on the microbes, but also the indirect treatment on the plasma-activated water (PAW) for the solution form. Herein, our results clearly revealed, for the first time based on our knowledge, the long-time stored effects of the plasma-modified plant tissue culture media.

Figures 6 and 7 depict the sets of KI-starch mixed samples which were treated by H_2, N_2, $H_2 + N_2$ and air plasmas captured at the standing time of 0, 5, 30 and 60 min after the treatment. All conditions were operated for 1 min of treatment time. The H_2-treated pattern showed a relatively small colored area immediately after the treatment (0 min). After that, the plasma-induced zone dramatically expanded just in 5 min later. This behavior confirms the role of plasma-produced RONS on the long-term effects in plasma-activated media which is specifically driven by H_2-derived species in this study. A slight change of the pattern between 30 and 60 min of standing times suggests that the post-treatment activity of RONS will eventually reach an equilibrium at the certain standing time. The area of the H_2-plasma clear zone in Fig. 5 was roughly 6.022 ± 1.014 cm^2 and approximately in line with the colored area of 7.956 ± 0.575 cm^2 at 60-min standing time. On account of the discussed plasma chemistry in the H_2 plasma, these characteristics are strongly suggested to be a result of highly diffusive H_2O_2. The plasma operated with N_2 feeding gas produced another unique distribution of plasma-produced RONS. The N_2-based chemistry, which at least included NO_3^--related species, seemed to be constantly unchanged during 60 min after the treatment. The result was in accordance with the antimicrobial effects, considering the size of the purple zone (3.127 ± 0.023 cm^2) and the bacteria-free area (3.157 ± 0.482 cm^2).

Because of the high mobility and cost-effectiveness, the air plasma has been considered as a good candidate for plasma agriculture. A dense point-like pattern surrounded by a broad distribution of the RONS convinces that other group of reactive species governed by O_2 and feeding humidity took a significant role. *The same order of* H_2O_2 *and* NO_3^- in air relative to N_2 plasmas tended to be ascribed to the air-derived species around the treatment point and resulted in comparable size between the bacterial inactivated area (3.519 ± 0.670 cm^2) and the reactive species distribution (3.618 ± 0.198 cm^2) after 60 min. In contrast, the outer pattern covered most of the Petri dish reasonably pointed to a consequence of a long-lived O_3 which is considerably stable in the atmospheric pressure and cannot sterilize the E. coli bacteria in the long term due to its low solubility in the gel. Surprisingly, the KI-starch mixed gel treated by the $H_2 + N_2$ plasma showed post-treatment behaviors analogous to its effective sterilization. A small point-like color was observed instantly after the treatment, which was almost identical to H_2-plasma condition, following by a substantial expansion for the next 60 min of standing time. The unsymmetric patterns were also observed in the previous section. The relatively large distribution resulted in 13.923 ± 1.483 cm^2 and was generally smaller than the bacteria-killing investigations with averaged area of 20.290 ± 2.158 cm^2. This provided compelling evidence for the key role of antimicrobial H_2O_2 which was overwhelmingly generated in $H_2 + N_2$ plasma as well as synergic effects *of* NO_3^- *and* NH_4^+*-related species.*

The KI-starch results explicitly supported that the post-treatment effects of the plasma-modified medium were caused by the further chemical reactions together with the confinement of plasma-generated species in the bulk region. To confirm this hypothesis, the H_2 $+N_2$ plasma which provided more deposition of the reactive species inside the gel compared with the air plasma was selected. The plasma was operated at the flow rate of 4 slm and gap distance of 5 mm. The 0.5% w/v gels were treated by the H_2+N_2 plasma for the same interval time of 1 min and then stored at room temperature for 0, 5, 10, 30, 45 and 60 min before spreading the *E. coli* in each sample. Next, the bacteria-embedded samples were incubated at 37 °*C* for 24 h and photographed. Figure 10 depicts the antimicrobial effects at different storage times of plasma-treated medium. It was clear that the plasma-modified effects were still effective in the long storage time up to 60 min after the treatment. The areas of the clear zone were explicitly storage-time independent which means that the plasma-activated area was governed by the steady-state size of the RONS distribution supported by the KI-starch probe. The spatial-unsymmetric distribution of RONS could arise from flow dynamics and surface curvature and result in a disproportional correlation between the clear zone and RONS distribution. Thus, the comparison of the equivalent radius (r_{eq}) which assumed that the plasma-activated area (A) is a circular shape ($A = \pi r_{eq}^2$) was proposed. All $H_2 + N_2$-treated gels resulted in the range of 2.712 to 3.005 cm of the equivalent radius. Figure 11b visualizes a plot of the equivalent radius as a function of a standing time for KI-starch mixed gel and storage time for bacteria-incubated gel. The tendency of the colored area induced by $H_2 + N_2$ plasma apparently reached an

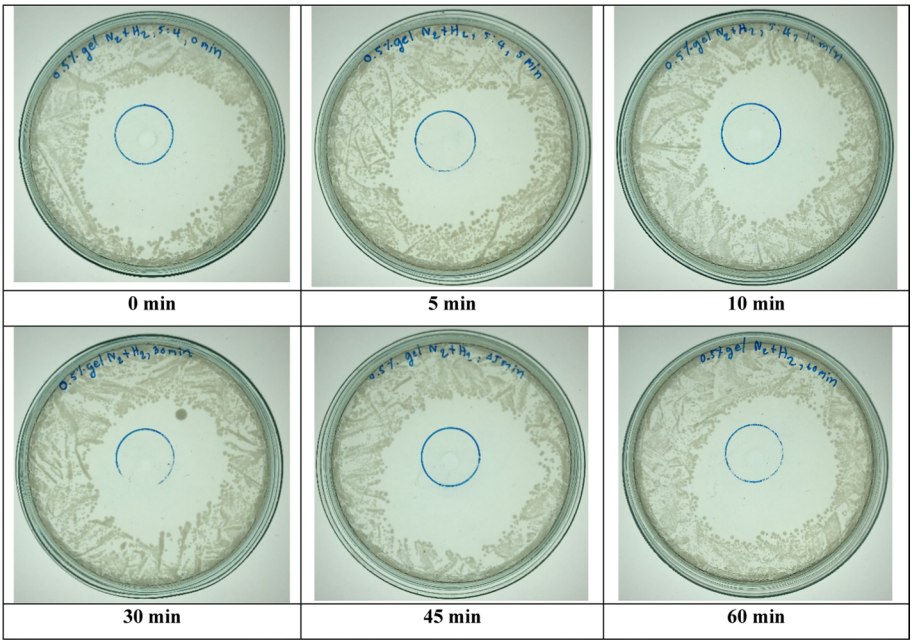

Fig. 10 Representative clear-zone images of *E. coli.* The nutrient agars were treated with H_2+N_2 plasma for 1 min and left for 0, 5, 10, 30, 45 or 60 min before the bacteria were spread onto the surface. After 1-day incubation, the images were taken, and the clear-zone area were measured. The quantitative results were shown in Fig. 11b. The nozzle gap was set at 5 mm. Flow rate was set at 4 slm. Experiments were done in triplicate

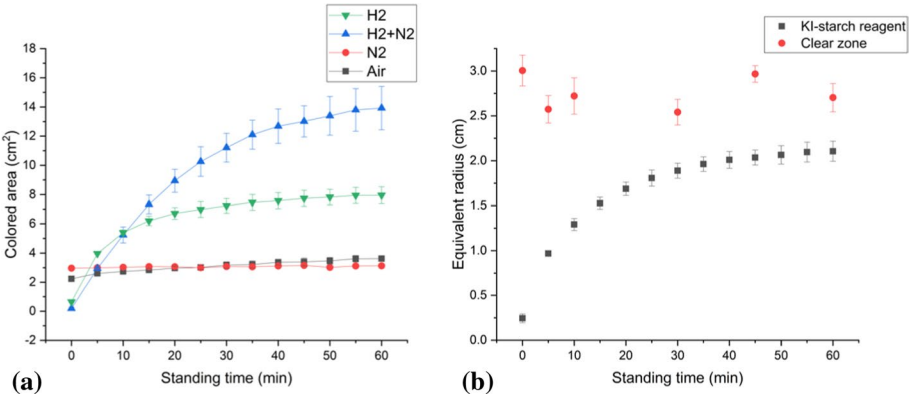

Fig. 11 **a** Colored area in KI-starch agar induced by plasma-generated RONS is plotted as a function of the standing time **b** The equivalent radius of the colored area on KI-starch mixed gel treated by H_2+N_2 plasma is presented together with the equivalent radius of the bacteria-free zone from different storage times. Experiments were done in triplicate

equilibrium state with $r_{eq} = 2.105 \pm 0.112$ cm which was practically confirmed the storage time independence. Notably, the plasma-storage effects were also shown to be active in a human body-like environment for 1 day of incubation whereas Shen et al. showed a significant reduction of antimicrobial effects with storage temperature up to 25℃ [52]. Therefore, it is reasonable to propose that the H_2+N_2 plasma can activate the long-term effects on the treated tissue culture media by depositing the reactive species in the bulk.

The dynamics of the post-treatment distribution of the plasma-generated RONS was quantitatively summarized in Fig. 11a. The KI-starch induced-colored area generally increased during the standing time since the chemical reactions can still take place and lead to the production and destruction of various secondary species. The behaviors of H_2 and $H_2 + N_2$ plasmas clearly showed a considerable increase from a point-like shape with the size less than 1 cm^2 and reached a steady-state size which was in the same order as clear zones. On the other hand, the colored area induced by air plasma slightly expanded from the initial size of 3.220 ± 0.249 cm^2 meanwhile the N_2-plasma induced species tended to stay constant over 60 min of standing time. These observations and calculations strongly provided a framework of the RONS' role in the long-lasting effects which strongly depends on the feeding gases. Although the KI-starch reagent is a non-specific probe for RONS produced by the plasma, this simple method can provide valuable information and serve as a basis for further investigations accompanied with other techniques such as RONS-specifically fluorescent probe or pH-dependent probe.

Effects of Indirect Plasma on Plant Tissue Culture

To study the effects of plasma indirect treatment on plant tissue culture, air plasma and H_2 +N_2 plasma were applied to treat the prepared culture medium before culturing process. *Drosera adelae* leaf explants were then observed for the day of shoot initiation and number of shoots produced. Results showed that plasma-treated samples gave off shoot faster than the controlled sample for approximately two days (18 and 16 days for control samples and treated samples, respectively), while H_2+N_2 or air plasma did not make a significant difference on the time required for the induction of shoot initiation (Fig. 12a). However,

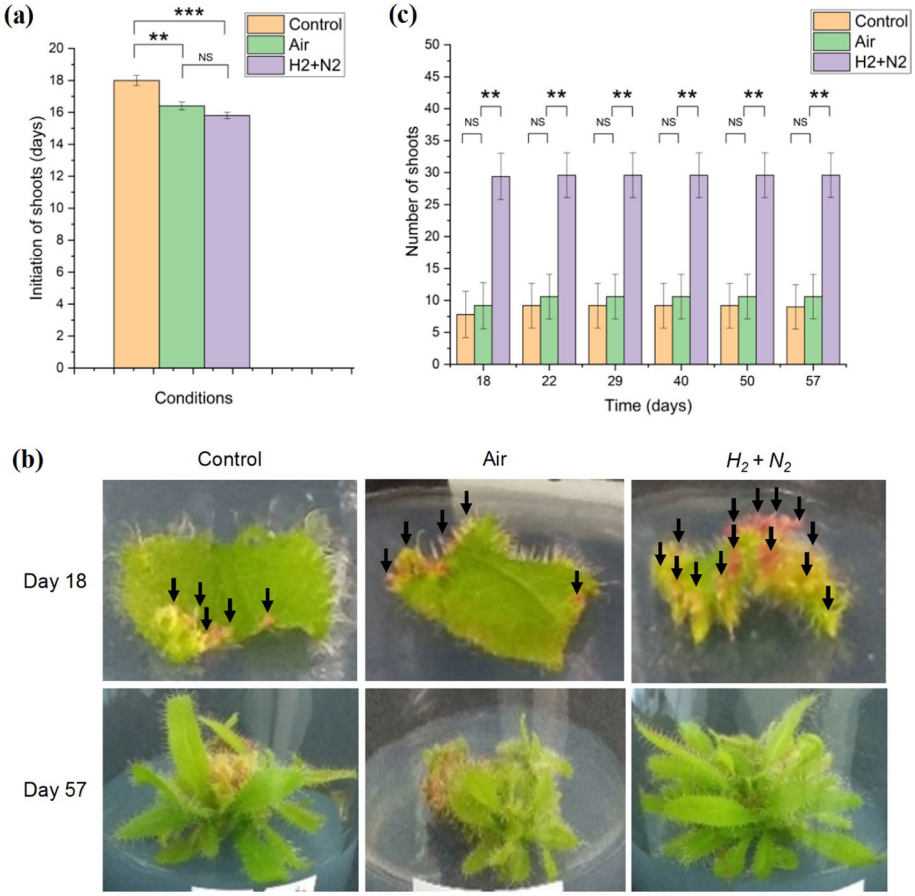

Fig. 12 Effects of indirect plasma treatment on *Drosera adelae* shoot initiation and shoot multiplication. After air and H_2+N_2 plasma treatment on tissue culture medium, leaf explants were cultured and observed. **a** Number of days required for shoot initiation in control, air plasma, and H_2+N_2 plasma treatment samples. **b** Representative pictures of *Drosera adelae* leaf explants with generated shoots (pointed with black arrows) at Day 18 and with young leaves at Day 58. **c** Numbers of generated shoot were counted and shown at the indicated days after culturing. Error bars indicate standard error (n = 5). NS, not significant. $*p<0.05$, $**p<0.01$, $***p<0.001$. The nozzle gap was set at 5 mm. Flow rate was set at 4 slm. Plasma treatment time = 1 min

for number of shoots generated, H_2+N_2 plasma (29.4 ± 6.8 shoots) induced the production of shoots approximately three-times more than air plasma (9.2 ± 2.3 shoots) or the control sample (7.8 ± 2.6 shoots, Fig. 12b, c).

Combining OES results and tissue culture results, since both $\mathbf{H_2}$+$\mathbf{N_2}$ and air plasma can induce early shooting, it is highly possible that $\mathbf{N_2}$ derivatives may be an important inducer for tissue culture shooting. Although we do not have concrete evidence or the directly comparable result indicating which species of $\mathbf{N_2}$ derivatives that induces shooting, it might be possible that nitrate plays a role in this regulation, considering from the preliminary RONS concentration results induced by plasma in DI water (Fig. S1). This speculation is supported by previous articles reporting nitrogen compounds have stimulatory effects on shoot organogenesis [53] and that high levels of nitrogen in both nitrate and ammonium

forms may positively affect the shoot generation [54]. Another research reported that the concentration and ratio of $\mathbf{NH_4^+}$ and $\mathbf{NO_3^-}$ also showed influences on shoot regeneration in *Aloe polyphylla* [55]. However, neither the exact mechanism of how nitrogen derivatives affect plant tissue culture shooting, nor the ratio of nitrate and ammonium best suited for the induction of shooting is discovered yet. Additional study on other potential derivatives of nitrogen such as nitrite ion ($\mathbf{NO_2^-}$) should also be done.

On the other hand, for the increased number of generated shoots, our results clearly show that components that can mainly be found in $\mathbf{H_2}$+$\mathbf{N_2}$ plasma but less in air plasma are responsible for this induction. From OES results (Fig. 4), $\mathbf{H_2}$ derivatives are a candidate for this induction. However, from the plasma-induced production of RONS in liquid phase (Fig. S1), ammonium is another candidate. Though the results from DI-water (Fig. S1) cannot be directly integrated and used to explain the incident in the semi-solid model, they provided us with some hints that would lead us to further investigation on the issue. Related to this, addition of hydrogen peroxide, one of the common hydrogen derivatives in liquid phase, into plant culture medium was reported to promote the generation of shoot in wheat and faba bean culture [56]. Although they are different plant species, intracellular regulation of plant is generally known to be relatively universal. Thus, this supports the importance of hydrogen derivatives in shoot multiplication. Still, there are also researches supporting the importance of nitrogen derivatives in shoot multiplication. Wada et al. [57] and Máximo et al. [58] both reported that ammonium and nitrate affected shoot multiplication in plants. To sum up, in-depth investigation is still needed to clarify which molecule affects shoot multiplication and what mechanism it affects.

Additionally, to choose the optimal feeding gases for agricultural applications, economic factors are needed to be considered. In terms of energy efficiency or the amount of produced chemical product per consumed energy or power, the electrical power results (Fig. 3) and the concentration of induced RONS in DI water (Fig. S1) were combined for calculation. $H_2 + N_2$ plasma was found to be outstanding. It induced the generation of 43.107 ± 1.962 g/kW h of H_2O_2 which was 12 times higher than the amount induced by H_2 plasma (3.670 ± 0.128 g/kW h). In case of NO_3^-, the production rate of 12.166 ± 5.928 g/kW h was also better than the O_2 or N_2 plasma group. Lastly, the highest concentration of NH_4^+ was also obtained when induced by $H_2 + N_2$ plasma (14.744 ± 2.668 g/kW h) as expected from the stoichiometric ratio of NH_3.

Taken together, nitrogen and hydrogen derivatives generated from the indirect plasma treatment can induce the generation of shoot and increase the number of shoots of *Drosera adelae* in tissue culture environment. However, the mechanism or appropriate amount or ratio of the compounds is still unclear and should be further investigated.

Conclusion

To standardize the application of cold atmospheric pressure plasma in agriculture, this study had investigated the 3-D diffusion and the deposition pattern of RONS in a semi-solid model. The association between the diffusion and bactericidal effects was also verified. Eventually, we introduced the application of the COMPACT Air Plasma Jet device on the preparation of agar-based plant tissue culture media for the purposes of sterilization and plant-growth stimulation. First, the pulse-averaged dissipated powers among different feeding gases including artificial air (20% O_2 + 80% N_2), air (RH 55–65%), N_2, H_2+ N_2 (75%H_2 + 25% N_2), H_2 and O_2 were examined. The dissipated powers were found to generally fall

in range of 0.71–0.98 W, except a drop in H_2 plasma to 0.57 ± 0.01 W accounted for lower breakdown voltage. In addition, the 3-time lower power of 0.24 ± 0.01 W in comparison with the humid air was observed in $H_2 + N_2$ plasma that was possibly thanks to the relative cross section, reduced effects of Penning ionization or secondary electronic emission coefficient. The gas temperatures of most feeding gases were also lower than human-body temperature (33.4–36.4 °C) but the exothermic nature of NH_3 formation was assumed to cause a significant rise of $H_2 + N_2$-fed gas temperature to 40.9 ± 0.3 °C. However, the thermal effects on the plasma-activated media (PAM) were insignificant. Second, the long-lasting antimicrobial effects of the treated gels were studied on *E. coli*. The medium that was plasma-treated 60-min prior to bacterial inoculation still showed bacterial inactivation effect. Remarkably, the $H_2 + N_2$ plasma provided the largest bacterial clear zone. Medium's softness as well as the gas flow rate significantly affected the distribution of RONS in a semi-solid medium. We consider the agar-based gel as a static water body that is encapsulated by a thin elastic layer of polymer. Thus, we proposed that the penetrated RONS from the gas phase will be deposited in the water bulk and account for the long-lasting effects of plasma activation. We proposed the dominant chemical pathways based on the gas–liquid solubility based on Henry's coefficient with supplementary results of the measurement of H_2O_2, NH_4^+ and NO_3^- concentration in DI water exposed to plasma. While, energy efficiency of $H_2 + N_2$ plasma crucially outperformed other feeding gases in the generation of all 3 detected species. Moreover, the deposition of plasma-induced RONS in agar was 3-D visualized by the KI-starch reagent. The colored area induced by KI-starch reagent was in accordance with the bacterial free zone. The RONS concentration per area should be considered to further clarify these observations. Lastly, the preliminary results on shoot multiplication and shoot initiation of *Drosera adelae* cultured on plasma-stimulated tissue culture medium were achieved. This study showed that $H_2 + N_2$-treated tissue culture media is a compelling candidate in terms of simultaneous effects of bacterial inactivation and plant growth promotion. These results demonstrate the feasibility of the cost-effective PAM in agricultural applications leading to food sustainability in the future.

Supplementary Information The online version contains supplementary material available at https://doi.org/10.1007/s11090-022-10228-4.

Acknowledgements This research work was partially supported by Chiang Mai University (CMU). K. Kosumsupamala gratefully acknowledges the Master's degree program in Applied Physics, Faculty of Science, Chiang Mai University, under the CMU Presidential scholarship. The authors also thank all staff members of the Plasma and Beam Physics Research Facility (PBP) for their efforts and support.

Availability of data and materials The data that support the findings of this study are available from the corresponding author upon reasonable request.

Declarations

Conflict of interest The authors have declared no conflicts of interest for this article.

References

1. Privat-Maldonado A, Schmidt A, Lin A, Weltmann KD, Wende K, Bogaerts A, Bekeschus S (2019) ROS from physical plasmas: redox chemistry for biomedical therapy. Oxid Med Cell Longev. https://doi.org/10.1155/2019/9062098

2. Sakudo A, Yagyu Y, Onodera T (2019) Disinfection and sterilization using plasma technology: fundamentals and future perspectives for biological applications. Int J Mol Sci. https://doi.org/10.3390/ijms20205216
3. Chen Z, Garcia G, Arumugaswami V, Wirz RE (2020) Cold atmospheric plasma for SARS-CoV-2 inactivation. Phys Fluids 32:111702. https://doi.org/10.1063/5.0031332
4. Bartis EAJ, Knoll AJ, Luan P, Seog J, Oehrlein GS (2016) On the interaction of cold atmospheric pressure plasma with surfaces of bio-molecules and model polymers. Plasma Chem Plasma Process 36:121–149. https://doi.org/10.1007/s11090-015-9673-2
5. Lee Y, Lee YY, Kim YS, Balaraju K, Mok YS, Yoo SJ, Jeon Y (2020) Enhancement of seed germination and microbial disinfection on ginseng by cold plasma treatment. J Ginseng Res. https://doi.org/10.1016/j.jgr.2020.12.002
6. Volin JC, Denes FS, Young RA, Park SMT (2000) Modification of seed germination performance through cold plasma chemistry technology. Crop Sci 40:1706–1718. https://doi.org/10.2135/cropsci2000.4061706x
7. Stoleru V, Burlica R, Mihalache G, Dirlau D, Padureanu S, Teliban G-C, Astanei D, Cojocaru A, Beniuga O, Patras A (2020) Plant growth promotion effect of plasma activated water on Lactuca sativa L. cultivated in two different volumes of substrate. Sci Rep 10:20920 . https://doi.org/10.1038/s41598-020-77355-w
8. Kučerová K, Henselová M, Slováková Ľ, Hensel K (2019) Effects of plasma activated water on wheat: germination, growth parameters, photosynthetic pigments, soluble protein content, and antioxidant enzymes activity. Plasma Process Polym 16:1800131. https://doi.org/10.1002/ppap.201800131
9. Iwata N, Gamaleev V, Hashizume H, Oh J, Ohta T, Ishikawa K, Hori M, Ito M (2019) Simultaneous achievement of antimicrobial property and plant growth promotion using plasma-activated benzoic compound solution. Plasma Process Polym 16:1900023. https://doi.org/10.1002/ppap.201900023
10. Goswami R, Sinha T, Ghosh K (2019) Drosera Sp: a critical review on phytochemical and ethnomedicinal aspect. Int J Pharm Bio Sci 9:596–601
11. Banasiuk R, Kawiak A, Królicka A (2012) In vitro cultures of carnivorous plants from the Drosera and Dionaea genus for the production of biologically active secondary metabolites. Biotechnologia 2:87–96. https://doi.org/10.5114/bta.2012.46572
12. Zhou R, Zhou R, Prasad K, Fang Z, Speight R, Bazaka K, Ostrikov K (2018) Cold atmospheric plasma activated water as a prospective disinfectant: the crucial role of peroxynitrite. Green Chem 20:5276–5284. https://doi.org/10.1039/C8GC02800A
13. Li S, Medrano Jimenez J, Hessel V, Gallucci F (2018) Recent progress of plasma-assisted nitrogen fixation research: a review. Processes 6:248. https://doi.org/10.3390/pr6120248
14. Thana P, Wijaikhum A, Poramapijitwat P, Kuensaen C, Meerak J, Ngamjarurojana A, Sarapirom S, Boonyawan D (2019) A compact pulse-modulation cold air plasma jet for the inactivation of chronic wound bacteria: development and characterization. Heliyon 5:e02455. https://doi.org/10.1016/j.heliyon.2019.e02455
15. Kawasaki T (2014) Visualization of the distribution of oxidizing substances in an atmospheric pressure plasma jet. IEEE Trans Plasma Sci 42:2482–2483. https://doi.org/10.1109/TPS.2014.2325038
16. Vacin EF, Went FW (1949) Some pH changes in nutrient solutions. Bot Gaz 110:605–613. https://doi.org/10.1086/335561
17. Ollegott K, Wirth P, Oberste-Beulmann C, Awakowicz P, Muhler M (2020) Fundamental properties and applications of dielectric barrier discharges in plasma-catalytic processes at atmospheric pressure. Chemie Ing Tech 92:1542–1558. https://doi.org/10.1002/cite.202000075
18. Radmilović-Radjenović M, Radjenović B, Matejčik Š, Klas M (2014) The breakdown phenomena in micrometer scale direct-current gas discharges. Plasma Chem Plasma Process 34:55–64. https://doi.org/10.1007/s11090-013-9488-y
19. Hassouba M, Mehanna E (2009) Electrical characteristics of (N2–H2) gas mixture DC glow discharge. Int J Phys Sci 4:713–721
20. Martínez H, Yousif FB (2008) Electrical and optical characterization of pulsed plasma of N2–H2. Eur Phys J D 46:493–498. https://doi.org/10.1140/epjd/e2008-00006-6
21. Farouk T, Farouk B, Staack D, Gutsol A, Fridman A (2007) Modeling of direct current microplasma discharges in atmospheric pressure hydrogen. Plasma Sources Sci Technol 16:619–634. https://doi.org/10.1088/0963-0252/16/3/023
22. Kawasaki T, Sato A, Kusumegi S, Kudo A, Sakanoshita T, Tsurumaru T, Uchida G, Koga K, Shiratani M (2016) Two-dimensional concentration distribution of reactive oxygen species transported through a tissue phantom by atmospheric-pressure plasma-jet irradiation. Appl Phys Express 9:1–5 . https://doi.org/10.7567/APEX.9.076202

23. He T, Liu D, Liu Z, Liu Z, Li Q, Rong M, Kong MG (2017) The mechanism of plasma-assisted penetration of NO 2—in model tissues. Appl Phys Lett 111:203702. https://doi.org/10.1063/1.4999366
24. Goff HD, Guo Q (2019) Chapter 1. The role of hydrocolloids in the development of food structure, pp 1–28
25. Stephen AM, Phillips GO, Williams PA (2016) Chapter 7. Agars. In: Food polysaccharides and their applications. CRC Press, Cambridge, pp 217–238
26. Kruszelnicki J, Lietz AM, Kushner MJ (2019) Atmospheric pressure plasma activation of water droplets. J Phys D Appl Phys 52:355207. https://doi.org/10.1088/1361-6463/ab25dc
27. Machala Z, Tarabová B, Sersenová D, Janda M, Hensel K (2019) Chemical and antibacterial effects of plasma activated water: correlation with gaseous and aqueous reactive oxygen and nitrogen species, plasma sources and air flow conditions. J Phys D Appl Phys 52:034002. https://doi.org/10.1088/1361-6463/aae807
28. Zhao Y, Patange A, Sun D, Tiwari B (2020) Plasma-activated water: physicochemical properties, microbial inactivation mechanisms, factors influencing antimicrobial effectiveness, and applications in the food industry. Compr Rev Food Sci Food Saf 19:3951–3979. https://doi.org/10.1111/1541-4337.12644
29. Khlyustova A, Labay C, Machala Z, Ginebra M-P, Canal C (2019) Important parameters in plasma jets for the production of RONS in liquids for plasma medicine: A brief review. Front Chem Sci Eng 13:238–252. https://doi.org/10.1007/s11705-019-1801-8
30. McClurkin JD, Maier D (2010) Half-life time of ozone as a function of air conditions and movement. Julius-Kühn-Archiv 381
31. Sysolyatina EV, Lavrikova AY, Loleyt RA, Vasilieva EV, Abdulkadieva MA, Ermolaeva SA, Sofronov AV (2020) Bidirectional mass transfer-based generation of plasma-activated water mist with antibacterial properties. Plasma Process Polym 17:2000058. https://doi.org/10.1002/ppap.202000058
32. Roeselová M, Vieceli J, Dang LX, Garrett BC, Tobias DJ (2004) Hydroxyl radical at the air−water interface. J Am Chem Soc 126:16308–16309. https://doi.org/10.1021/ja045552m
33. Becker KH, Kleffmann J, Martin Negri R, Wiesen P (1998) Solubility of nitrous acid (HONO) in ammonium sulfate solutions. J Chem Soc Faraday Trans 94:1583–1586. https://doi.org/10.1039/a800458g
34. Clegg SL, Brimblecombe P (1990) Equilibrium partial pressures and mean activity and osmotic coefficients of 0–100% nitric acid as a function of temperature. J Phys Chem 94:5369–5380. https://doi.org/10.1021/j100376a038
35. Sander R (2015) Compilation of Henry's law constants (version 4.0) for water as solvent. Atmos Chem Phys 15:4399–4981. https://doi.org/10.5194/acp-15-4399-2015
36. Malik MA (2016) Nitric oxide production by high voltage electrical discharges for medical uses: a review. Plasma Chem Plasma Process 36:737–766. https://doi.org/10.1007/s11090-016-9698-1
37. Goldstein S, Lind J, Merényi G (2005) Chemistry of peroxynitrites as compared to peroxynitrates. Chem Rev 105:2457–2470. https://doi.org/10.1021/cr0307087
38. Reuter S, Winter J, Iseni S, Schmidt-Bleker A, Dunnbier M, Masur K, Wende K, Weltmann K-D (2015) The influence of feed gas humidity versus ambient humidity on atmospheric pressure plasma jet-effluent chemistry and skin cell viability. IEEE Trans Plasma Sci 43:3185–3192. https://doi.org/10.1109/TPS.2014.2361921
39. Rezaei F, Vanraes P, Nikiforov A, Morent R, De Geyter N (2019) Applications of plasma-liquid systems: a review. Mater (Basel, Switzerland). https://doi.org/10.3390/ma12172751
40. Xu L, Yepez X, Applegate B, Keener KM, Tao B, Garner AL (2020) Penetration and microbial inactivation by high voltage atmospheric cold plasma in semi-solid material. Food Bioprocess Technol 13:1688–1702. https://doi.org/10.1007/s11947-020-02506-w
41. Haruyama T, Namise T, Shimoshimizu N, Uemura S, Takatsuji Y, Hino M, Yamasaki R, Kamachi T, Kohno M (2016) Non-catalyzed one-step synthesis of ammonia from atmospheric air and water. Green Chem 18:4536–4541. https://doi.org/10.1039/C6GC01560C
42. Mitsugi F, Kusumegi S, Kawasaki T (2019) Visualization of ROS distribution generated by atmospheric plasma Jet. IEEE Trans Plasma Sci 47:1057–1062. https://doi.org/10.1109/TPS.2018.2858807
43. Ghimire B, Szili EJ, Lamichhane P, Short RD, Lim JS, Attri P, Masur K, Weltmann K-D, Hong S-H, Choi EH (2019) The role of UV photolysis and molecular transport in the generation of reactive species in a tissue model with a cold atmospheric pressure plasma jet. Appl Phys Lett 114:093701. https://doi.org/10.1063/1.5086522
44. Uhm HS, Ki SH, Baik KY, Choi EH (2018) Influence of oxygen on generation of reactive chemicals from nitrogen plasma jet. Sci Rep 8:9318. https://doi.org/10.1038/s41598-018-27473-3

45. He T, Liu D, Xu H, Liu Z, Xu D, Li D, Li Q, Rong M, Kong MG (2016) A 'tissue model' to study the barrier effects of living tissues on the reactive species generated by surface air discharge. J Phys D Appl Phys 49:205204. https://doi.org/10.1088/0022-3727/49/20/205204
46. Liu D, He T, Liu Z, Wang S, Liu Z, Rong M, Kong M (2018) Spatial-temporal distributions of ROS in model tissues treated by a He+O 2 plasma jet. Plasma Process Polym 15:1800057. https://doi.org/10.1002/ppap.201800057
47. Boselli M, Colombo V, Ghedini E, Gherardi M, Laurita R, Liguori A, Sanibondi P, Stancampiano A (2014) Schlieren high-speed imaging of a nanosecond pulsed atmospheric pressure non-equilibrium plasma jet. Plasma Chem Plasma Process 34:853–869. https://doi.org/10.1007/s11090-014-9537-1
48. Pei X, Ghasemi M, Xu H, Hasnain Q, Wu S, Tu Y, Lu X (2016) Dynamics of the gas flow turbulent front in atmospheric pressure plasma jets. Plasma Sources Sci Technol 25:035013. https://doi.org/10.1088/0963-0252/25/3/035013
49. Davidson, TA (1993) A simple and accurate method for calculating viscosity of gaseous mixtures. United States. https://www.osti.gov/biblio/6129940
50. Yue Y, Pei X, Gidon D, Wu F, Wu S, Lu X (2018) Investigation of plasma dynamics and spatially varying O and OH concentrations in atmospheric pressure plasma jets impinging on glass, water and metal substrates. Plasma Sources Sci Technol 27:64001. https://doi.org/10.1088/1361-6595/aac618
51. Simoncelli E, Stancampiano A, Boselli M, Gherardi M, Colombo V (2019) Experimental investigation on the influence of target physical properties on an impinging plasma jet. Plasma 2:369–379. https://doi.org/10.3390/plasma2030029
52. Shen J, Tian Y, Li Y, Ma R, Zhang Q, Zhang J, Fang J (2016) Bactericidal effects against *S. aureus* and physicochemical properties of plasma activated water stored at different temperatures. Sci Rep 6:28505 . https://doi.org/10.1038/srep28505
53. Shetty K, Asano Y, Oosawa K (1992) Stimulation of in vitro shoot organogenesis in Glycine max (Merrill.) by allantoin and amides. Plant Sci 81:245–251. https://doi.org/10.1016/0168-9452(92)90048-Q
54. Phillips GC, Garda M (2019) Plant tissue culture media and practices: an overview. Vitr Cell Dev Biol - Plant 55:242–257. https://doi.org/10.1007/s11627-019-09983-5
55. Ivanova M, Van Staden J (2009) Nitrogen source, concentration, and NH4 +:NO3—ratio influence shoot regeneration and hyperhydricity in tissue cultured Aloe polyphylla. Plant Cell Tissue Organ Cult 99:167–174. https://doi.org/10.1007/s11240-009-9589-8
56. Szechyńska-Hebda M, Skrzypek E, Dąbrowska G, Wędzony M, van Lammeren A (2012) The effect of endogenous hydrogen peroxide induced by cold treatment in the improvement of tissue regeneration efficiency. Acta Physiol Plant 34:547–560. https://doi.org/10.1007/s11738-011-0852-3
57. Wada S, Niedz RP, Reed BM (2015) Determining nitrate and ammonium requirements for optimal in vitro response of diverse pear species. Vitr Cell Dev Biol - Plant 51:19–27. https://doi.org/10.1007/s11627-015-9662-4
58. Máximo WPF, Santos PAA, Mendonça EG, Santos BR, Paiva LV (2015) Nitrate (NO3-) and ammonium (NH4+) ratios for propagation of Eucalyptus hybrid in two different in vitro cultivation systems. Aust J Crop Sci 9:1242–1248